Numerical investigation of heat transfer using impinging jets on triangular and square ribbed roughened walls

Article · January 2017

CITATIONS
0

READS
20

4 authors, including:

Sinan Caliskan
Hitit University
49 PUBLICATIONS **370** CITATIONS
SEE PROFILE

Mustafa Kilic
Adana Science and Technology University
37 PUBLICATIONS **44** CITATIONS
SEE PROFILE

Isı Bilimi ve Tekniği Dergisi, 37, 1, 13-24, 2017
J. of Thermal Science and Technology

ISSN 1300-3615

NUMERICAL INVESTIGATION OF HEAT TRANSFER USING IMPINGING JETS ON TRIANGULAR AND SQUARE RIBBED ROUGHENED WALLS

Tamer ÇALIŞIR, Sinan ÇALIŞKAN***, Mustafa KILIÇ**** and Şenol BAŞKAYA*,****
*Near East University, Faculty of Eng., Turkish Republic of Northern Cyprus, 99138 Lefkoşa/KKTC
**Gazi University Faculty of Engineering Mechanical Engineering Dept. 06570 Maltepe, Ankara,
tamercalisir@gazi.edu.tr, baskaya@gazi.edu.tr
***Hitit University Faculty of Engineering Mechanical Engineering Dept. 19030, Çorum
sbycaliskan@gmail.com
****Adana Science and Technology Univ. Faculty of Eng. and Natural Sci. Mechanical Eng. Dept. 01180, Adana
mustafaatakilic@gmail.com

(Geliş Tarihi: 04.11.2015, Kabul Tarihi: 19.07.2016)

Abstract: This paper presents a heat removal study on triangular and square ribbed surfaces under an array of impinging air jets. The investigation was carried out using nozzles with a 7x3 rectangular array of circular jets. The effect of Re number, jet-to-plate distance, and rib arrangement on heat transfer and fluid flow characteristics was examined numerically. Two arrangements have been studied. Arrangement A considers the situation when the cooling jets are directed towards the ribs, while arrangement B considers the situation when the jets are directed towards the centre line of the cavity between two ribs. Wall jets of neighboring jets have a stronger interaction with increasing Reynolds number. The lowest and highest local heat transfer for all rib geometries was obtained for H/d=8 and H/d=4-6, respectively. On triangular ribbed surfaces the stagnation point Nusselt number values for arrangement A are significantly higher than the stagnation point Nusselt numbers for arrangement B.
Keywords: Impinging jet, Heat transfer, Rib, CFD.

ÜÇGEN VE KARE KANATÇIKLI YÜZEYLER ÜSTÜNDEKİ ÇARPAN AKIŞKAN JETLER KULLANILARAK ISI TRANSFERİNİN SAYISAL İNCELENMESİ

Özet: Bu çalışmada, çoklu çarpmalı jetler kullanarak üçgen ve kare kanatçıklı yüzeylerin soğutulması sunulmuştur. 7x3 olarak dikdörtgen dizilime sahip dairesel jetler kullanılarak çalışma gerçekleştirilmiştir. Re sayısının, jet-plaka mesafesinin ve kanatçık diziliminin akış ve ısı transferine olan etkisi sayısal olarak irdelenmiştir. İki kanatçık dizilimi incelenmiştir. A dizilimi jetlerin doğrudan kanatçıkların üstüne çarpmasını, B dizilimi ise jetlerin iki kanatçığın ortasına çarpması durumlarını göstermektedir. İki komşu jetin duvar jetleri artan Re sayısı ile daha şiddetli bir şekilde etkileşmektedir. En yüksek ve en düşük ortalama ısı transferi değerleri tüm kanatçık geometrilerinde sırasıyla H/d=8 ve H/d=4-6 oluşmaktadır. Üçgen kanatçıklı yüzeylerde çarpma noktası Nu sayısı değerleri A düzenlemesinde B düzenlemesine göre daha yüksek olduğu görülmüştür.
Anahtar Kelimeler: Çarpmalı jet, ısı transferi, Kanatçık, HAD.

NOMENCLATURE

d	Nozzle diameter [mm]
e	Rib height [mm]
e/d	Dimensionless rib height
H	Jet-to-plate distance [mm]
H/d	Dimensionless jet-to-plate distance
h	Local heat transfer coefficient [W/m^2.K]
I	Turbulence intensity
k	Turbulence kinetic energy [m^2/s^2]
k	Conduction coefficient [W/m.K]
L	Plate length [mm]
l	Distance between ribs [mm]
Nu	Local Nusselt number [q".d/k.(T_w-T_j)]
q"	Heat flux [W/m^2]
p	Pressure [Pa]
Pr	Prandtl number
Re	Reynolds number [=w_j.d/ν]
Re_t	Turbulence Reynolds number
Re_z	Turbulence Reynolds number near the wall
s	Rib width [mm]
T	Temperature [°C]
T_j	Jet inlet temperature [°C]
T_w	Impingement plate local temperature [°C]
u_τ	Friction velocity
u,v,w	Velocity components [m/s]
W	Plate width [mm]
w_j	Jet inlet velocity [m/s]
y^+	Dimensionless distance from the wall

Greek Symbols

ε	Dissipation rate of turbulent kinetic energy
μ	Dynamic viscosity [kg/m.s]
μ_t	Eddy viscosity [kg/m.s]
ν	Kinematic viscosity [m^2/s]
ρ	Density [kg/m^3]
σ_k	Turbulent Prandtl number for k

σ_ε Turbulent Prandtl number for ε
τ_w Shear stress at the wall [Pa]

Subscript

j Jet inlet
w Wall

Superscript

‘ Fluctuation
¯ Mean

INTRODUCTION

Impingement heat transfer is considered as an attractive heat transfer enhancement technique and has been applied to engineering problems which require high heat and mass transfer efficiency for cooling, heating, or desiccation. Impingement cooling technique have been used in various industries as an efficient approach to dissipate heat for protecting components that experience either high heat flux or high temperatures.

A vast amount of literature is dedicated to impinging jets. The effect of jet-to-jet spacing on heat transfer was investigated experimentally (Katti and Prabhu, 2008, 2009a, 2009b; San and Lai, 2001). Slot-air-jet impingement cooling flow and heat transfer along triangular and square rib roughened walls was studied experimentally by Gau and Lee (1992, 2000). Lytle and Webb (1994) examined experimentally the local heat transfer characteristics of air jet impingement at nozzle-plate spacing of less than one nozzle diameter. Multiple jet impingement on surfaces with different rib geometries was investigated experimentally (Caliskan, 2013; Caliskan and Baskaya, 2012). Effect of jet geometry of multiple and single jet impingement on heat transfer was examined experimentally (Caliskan et al., 2014; Koseoglu and Baskaya, 2010). San and Shiao (2006) dealed with the effects of jet plate size and jet height on the heat transfer characteristics for a confined circular air jet. Wang et al. (2005) provided a new database of heat transfer coefficients on a jet impingement target surface, using an 8x11 array of impinging jets. Many investigations on impinging jets and their applications were performed numerically and can be found in the literature. Miao et al. (2009) investigated the fluid flow and heat transfer characteristics of round jet arrays impinging orthogonally on a flat-plate with confined walls at different crossflow orientations. Low-Reynolds number flows and wall treatment was investigated and different low-Reynolds number turbulence models were examined (Patel et al., 1985; Bredberg and Davidson, 2004).

From the literature survey it can be concluded that jet arrays and surface roughness are quite important on impingement flow and heat transfer. However, it appears that there is only little information available on the effect of multiple jets impinging on ribbed surfaces from a fluid dynamics perspective.

In this article, we mainly focus our attention on how the heat transfer on the impingement plate can be affected by the following aspects: The Reynolds number (Re), the dimensionless jet-to-plate distance (H/d), dimensionless rib height (e/d), rib geometry and rib arrangement. The main objective of this study was to investigate the possibility to affect the heat transfer and fluid flow characteristics over the triangular and square rib-roughened surface, and to observe the cooling heat transfer enhancement. With these changes on the plate surface, we will seek the configuration that provides the highest heat exchange in comparison with a flat plate, when the same type of jet and jet-to-plate distance and Reynolds number are used.

MATHEMATICAL FORMULATION AND NUMERICAL MODEL

In this section, the numerical description of the problem under investigation is presented. Mathematical formulation, problem description, solution technique, boundary conditions, data reduction, and validation of the numerical model are described.

Problem Description

In the present numerical study, local and average heat transfer characteristics on a triangular and square ribbed surface under an in-line array of impinging jets, which are arranged as 7x3 circular jets were investigated using PHOENICS CFD code. For all the ribbed surfaces, simulations were performed for Re=3000-10000, and H=2d-8d. In addition, two rib arrangements were investigated for dimensionless rib heights of e/d=0.333-0.667. Arrangement A considers the situation when the cooling jets are directed towards the ribs, while arrangement B considers the situation when the jets are directed towards the centre line of the cavity between two ribs. Constant heat flux ($q'' = 1200 W/m^2$) was implemented on the impingement plate which is 210 mm long and 90 mm wide. The nozzles have a diameter (d) of 6 mm and are impinging vertically on the impingement plate. The distance between jets in the lengthwise as well as in the crosswise directions were chosen as 5d, which was selected in consideration of the study of Katti and Prabhu (2008, 2009a, 2009b).

Figure 1 shows a schematic of the impinging jet configuration as well as the rib arrangement and rib geometries used in this study. Implemented boundary conditions are also presented in this figure.

Turbulence Model Selection and Mathematical Formulation

In impinging jet studies eddy viscosity and Reynolds stress turbulence models are widely used. Wang and Mujumdar (2005) tested several low Reynolds k-ε models for confined turbulent slot jets. They obtained that the turbulence models were able to predict the general shape of the Nu number distribution but over predicted stagnation point values. In the present numerical study, because of the above stated reasons and also due to its simplicity and availability in the used CFD code, the Lam-Bramhorst low Reynolds number k-ε model was chosen. This model differs from the standard high-Reynolds-number turbulence model in that the empirical coefficients C_μ, C_1 and C_2 are multiplied by damping functions which help to reduce the excessive kinetic energy production and over prediction in the stagnation region. The continuity, Reynolds averaged momentum and time averaged energy equations governing 3-dimensional steady flow of air with constant properties are shown in Eq. (1) – (3), respectively.

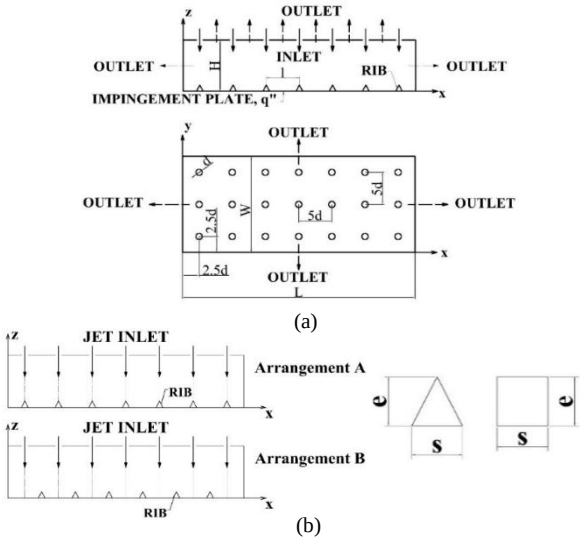

Figure 1. Problem geometry (a) boundary conditions, (b) Rib arrangements and rib geometries

$$\frac{\partial U_i}{\partial x_i} = 0 \tag{1}$$

$$\rho U_i \frac{\partial U_j}{\partial x_i} = -\frac{\partial P}{\partial x_j} + \frac{\partial}{\partial x_i}\left[\mu\left(\frac{\partial U_i}{\partial x_j} + \frac{\partial U_j}{\partial x_i}\right) - \rho\overline{u_i' u_j'}\right] \tag{2}$$

$$\rho c_p U_i \frac{\partial T}{\partial x_i} = \frac{\partial}{\partial x_i}\left[k\frac{\partial T}{\partial x_i} - \rho c_p \overline{u_i' T'}\right] \tag{3}$$

The transport equations of the k-ε model are adapted to consider the low Reynolds effects, and the model is found by multiplying the empirical coefficients C_μ, $C_{1\varepsilon}$, $C_{2\varepsilon}$ of the standard model with damping functions. The transport equations of the model are as follows:

$$\rho U_i \frac{\partial k}{\partial x_i} = \frac{\partial}{\partial x_i}\left[\left(\mu + \frac{\mu_t}{\sigma_k}\right)\frac{\partial k}{\partial x_i}\right] + \mu_t\left(\frac{\partial U_i}{\partial x_j} + \frac{\partial U_j}{\partial x_i}\right)\frac{\partial U_i}{\partial x_j} - \rho\varepsilon \tag{4}$$

$$\rho U_i \frac{\partial \varepsilon}{\partial x_i} = \frac{\partial}{\partial x_i}\left[\left(\mu + \frac{\mu_t}{\sigma_\varepsilon}\right)\frac{\partial \varepsilon}{\partial x_i}\right] + f_1 C_1 \mu_t \frac{\varepsilon}{k}\left(\frac{\partial U_i}{\partial x_j} + \frac{\partial U_j}{\partial x_i}\right)\frac{\partial U_i}{\partial x_j} - f_2 C_2 \rho \frac{\varepsilon^2}{k} \tag{5}$$

The turbulent kinetic viscosity is expressed as:

$$\mu_t = f_\mu C_\mu \rho \frac{k^2}{\varepsilon} \tag{6}$$

C_μ, $C_{1\varepsilon}$, $C_{2\varepsilon}$ are empirical constants of the model and σ_k and σ_ε are turbulent Prandtl number for k and ε, respectively. The values of the constants are given below.

$$\sigma_k = 1.00;\quad \sigma_\varepsilon = 1.314;\quad C_1 = 1.44;\quad C_2 = 1.92;\quad C_\mu = 0.09 \tag{7}$$

The damping functions of the Lam-Bramhorst low Reynolds number k-ε model are presented in the equations below.

$$f_\mu = \left[1 - exp(-0.0165 Re_z)\right]^2\left(1 + \frac{20.5}{Re_t}\right) \tag{8}$$

$$f_1 = \left(1 + \frac{0.05}{f_\mu}\right)^3 \tag{9}$$

$$f_2 = 1 - exp\left(-Re_t^{\,2}\right) \tag{10}$$

where,

$$Re_t = \frac{\rho k^2}{\mu\varepsilon} \tag{11}$$

$$Re_z = \frac{\rho k^{1/2} z}{\mu} \tag{12}$$

Solution Technique

The steady state problem was solved in cartesian coordinates. The continuity, momentum and energy equations for a three dimensional incompressible turbulent flow has been solved using appropriate boundary conditions. For the pressure correction process along with the solution procedure for the hydrodynamic equations the code employs the SIMPLEST algorithm. A staggered grid arrangement was used and for the discretization of convective-diffusive transport, the hybrid scheme is the default scheme within the code.

Boundary Conditions

The boundary conditions of this study are shown on Figure 1 (a) and summarized in Table 1. Only the inlet sections of the 7x3 jet array were modelled. Outlet boundary conditions were implemented around the jets and at the four sides of the geometry. On the solid walls the no-slip condition was accommodated and velocities were taken as zero. Constant wall heat flux was applied on the impingement plate. The ribs were modelled without any conjugate heat transfer. Flow and heat transfer was modelled for steady-state conditions. Radiation effects were not considered.

As can be seen from Table 1 the boundary conditions for k and ε are implemented in that way because the low Reynolds number turbulence model does not use wall functions. Jet inlet temperature was taken as 20°C. In contrary to the wall boundary conditions, the same boundary conditions for k and ε can be applied at the outlet for the low Reynolds turbulence model as well as the standard model. It was accepted that the outlet is to the atmosphere.

Validation of the Numerical Results

Linear algebraic equations which are obtained from the finite volume integration of partial differential equations are solved iteratively, and convergence was considered as being

achieved when these residuals become less than 10^{-7}, which was the case for most of the dependent variables. Iterative convergence was also checked by terminating the solution only then the progressive single cell values of pressure, velocity, and temperature showed little change per iteration as the calculation progressed. In addition, checks for the achievement of a final solution were made based on the conservation of mass, momentum and energy. Solutions were obtained for iteration and grid independency checks. It was seen that the solution becomes almost independent after 1500 iterations so the optimum iteration number was selected as 2000. A systematic grid independence study was performed to obtain an optimum mesh number. The convergence of the strip-averaged Nusselt number distribution under the mid-row jets for different mesh numbers are shown in Figure 2 (a). The optimum mesh number in the x-y-z planes was selected as 165-55-45, respectively. Because no wall functions were used in the implemented turbulence model, grids were refined in the jet region and close to the impingement plate, and the necessary number of nodes are placed within the viscous sublayer. Hence the y^+ value to the first node next to the wall was obtained in the order of 1.

For an estimate on the numerical accuracy of the computed results, a mesh sensitivity analysis was performed before comparing the numerical results with experimental data. An established method recommended by the Fluids Engineering Division of ASME (Celik et. al, 2008) is chosen. The resulting grid convergence index (GCI) method can be regarded as a procedure for uniform reporting of grid refinement studies. The method yields discretization error bands for the investigated variable, and thus represents a sophisticated quantification of mesh dependency. The changes in the mean y^+ values obtained from the sensitivity analysis are presented in Table 2, where x-y-z represents the mesh numbers in the x, y and z directions, respectively. This shows that the generated grid is satisfactory for the implemented turbulence model. The local discretization error distribution is shown in Figure 2 (b). These are calculated by applying the GCI method to the strip-averaged Nu number distribution along the mid-row jets. The overall discretization errors are below 9%. However, considering the complexity of the configuration, the overall result of the mesh sensitivity analysis is considered to be satisfying. The generated mesh of the whole geometry is shown on Figure 3.

The y^+ formula is shown below.

$$y^+ = \frac{u_\tau z}{\nu} \tag{13}$$

where,

$$u_\tau = \sqrt{\frac{\tau_w}{\rho}} \tag{14}$$

The numerical results were validated with the experimental study of Katti and Prabhu (2009) for Re=3000-10000, H/d=2.0, streamwise jet-to-jet distance of 5d and a span wise jet-to-jet distance of 4d. Relevant comparisons are presented in Figure 4. Validation was performed for strip-averaged Nusselt number values and local Nusselt number values. It was observed that the numerical results are to a large extent in agreement with the experimental results of Katti and Prabhu (2009). As can be seen, the numerical results were able to predict the Nu number profile in strip-averaged distributions. Also the local Nusselt number distributions show a good agreement with the experimental data. However, at x/d=22.5 the numerical results have under predicted the local Nusselt number values. This was interpreted as an effect due to air entraining in the computational domain and deteriorates the heat transfer. This occurs due to the turbulence model which could not optimally solve the impingement point heat transfer with entrainment, which is not the case for the experiment.

Table 1. Boundary Conditions

	U	V	W	T	k	ε
Inlet	U=0	V=0	$W=w_j$	$T=T_j$	$(I_j w_j)^2$	$(C_\mu C_d)^{3/4} k^{3/2} L$
Wall	U=0	V=0	W=0	q"=specified	k=0	$\partial\varepsilon/\partial z=0$
Outlet (x)	$\partial U/\partial x=0$	$\partial V/\partial x=0$	$\partial W/\partial x=0$	$\partial T/\partial x=0$	$\partial k/\partial x=0$	$\partial\varepsilon/\partial x=0$
Outlet (y)	$\partial U/\partial y=0$	$\partial V/\partial y=0$	$\partial W/\partial y=0$	$\partial T/\partial y=0$	$\partial k/\partial y=0$	$\partial\varepsilon/\partial y=0$
Outlet (z)	$\partial U/\partial z=0$	$\partial V/\partial z=0$	$\partial W/\partial z=0$	$\partial T/\partial z=0$	$\partial k/\partial z=0$	$\partial\varepsilon/\partial z=0$

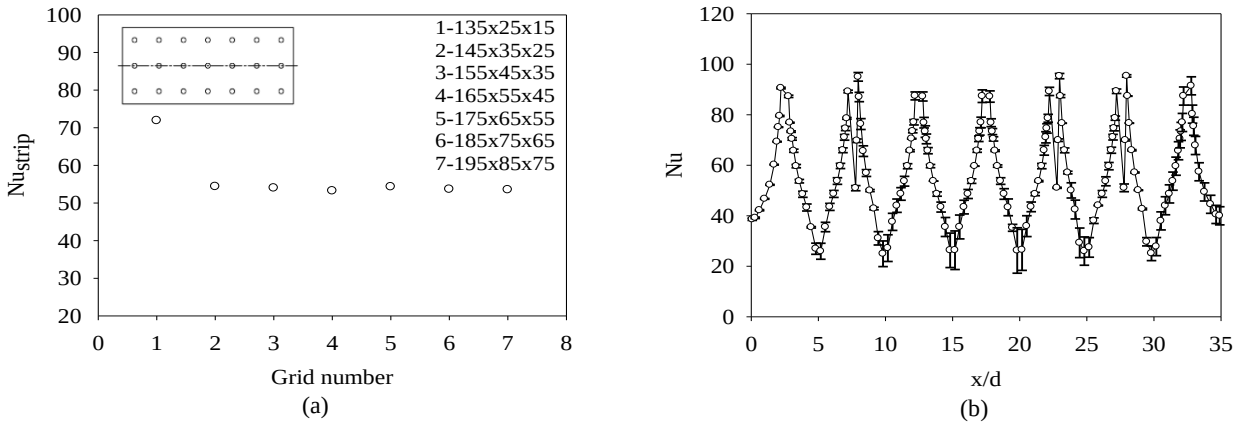

(a) (b)

Figure 2. Grid independency analysis at Re=10000, H/d=2.0 and e/d=0.5 (a) strip averaged Nu number, (b) GCI error band for the mid row Nu number distribution (fine grid)

Table 2. Mesh sensitivity analysis

Mesh	N (x-y-z)	Mean y^+
1	135x25x15	0.880
2	145x35x25	0.516
3	155x45x35	0.203
4	165x55x45	0.213
5	175x65x55	0.149
6	185x75x65	0.100
7	195x85x75	0.069

Data Reduction

The impingement plate surface temperature was obtained for steady state flow and heat transfer conditions under a constant jet inlet temperature (T_j). In this study, the impingement cooling effect data is mainly represented by local Nusselt (Nu) numbers, strip-averaged Nusselt (Nu_{strip}) numbers, and the area-averaged Nusselt (Nu_{ave}) numbers on the target plate. The Nusselt number values were obtained using the equations given below:

$$Nu = \frac{q''.d}{k(T_w - T_j)};\ Nu_{strip} = \frac{\int Nu dx}{L};\ Nu_{ave} = \frac{\iint Nu dx dy}{WL} \quad (15)$$

where q" is the constant heat flux of the impingement plate, d is the diameter of the jet, k is the thermal conductivity of air, T_w and T_j are the wall temperature and jet inlet temperature, respectively. L and W are the length and width of the impingement plate, respectively. In addition, the Reynolds number was calculated as follows:

$$Re = \frac{w_j.d}{\nu} \quad (16)$$

where w_j represents the jet inlet velocity and ν shows the kinematic viscosity of air.

RESULTS AND DISCUSSION

In this section, numerical results of the effects of rib geometry, rib arrangement, Reynolds number and jet-to-plate distance on impinging jet heat transfer are presented. Simulations were performed for triangular and square ribbed surfaces. Ribs were modelled as e=s. Another point in this presentation is that when nothing is mentioned the results are presented for arrangement A of ribs.

In general, the impinging jet flow along a ribbed wall is significantly different from that along a flat plate. Velocity vector distributions for triangular and square ribbed surfaces are presented in Figure 5. Results are presented for Re=3000-10000, H/d=2.0, e/d=0.5 for Arrangement A. Due to the symmetrical flow structure only half of the flow field is shown. It is observed that the wall jets of neighboring jets have a stronger interaction with increasing Reynolds number. For H/d=2.0 and e/d=0.5, the jets separate before impingement for both rib geometries with increasing Re number.

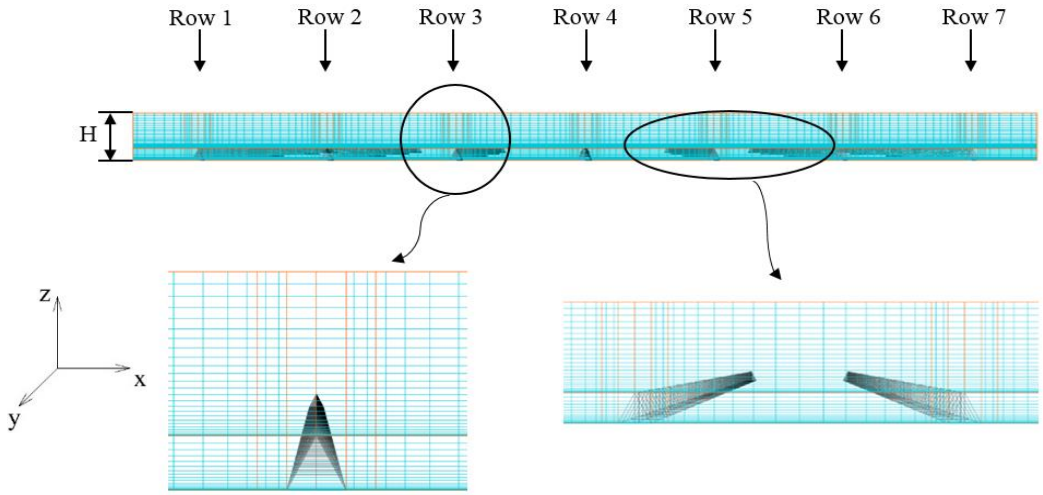

Figure 3. Generated mesh structure

This is attributed to the fact that the pressure over the rib is significantly higher with increasing Re number and formation of an air bubble which prevents the air jet from impinging on the rib. However, this fact is also observed at Re=3000 for square ribs. This situation occurs because the triangular shape of ribs can form cavities more widely open than the square ribs. Although the results for higher jet-to-plate distances are not shown in this paper it was observed that the jet impinges with a lower velocity on the surface, and the wall jets flow with a lower velocity over the ribbed surface, which in turn has a significant effect on the wall jet interaction between neighboring jets. In addition, it was observed that the recirculation after impingement was decreased.

The pressure distribution on the impingement plate was also investigated and the results under the mid-plane jets for Re=3000-10000 and on triangular and square ribbed surfaces are shown on Figure 6. As can be seen, the pressure distribution for the triangular ribbed surface at the stagnation point is higher for all Re numbers. This is attributed to the separation of the jet flow over the square ribs before impingement.

After the flow field investigation heat transfer results are presented. Local as well as average Nusselt number distributions were calculated and reported. In the last part of this section correlations obtained for area-averaged Nu numbers are presented.

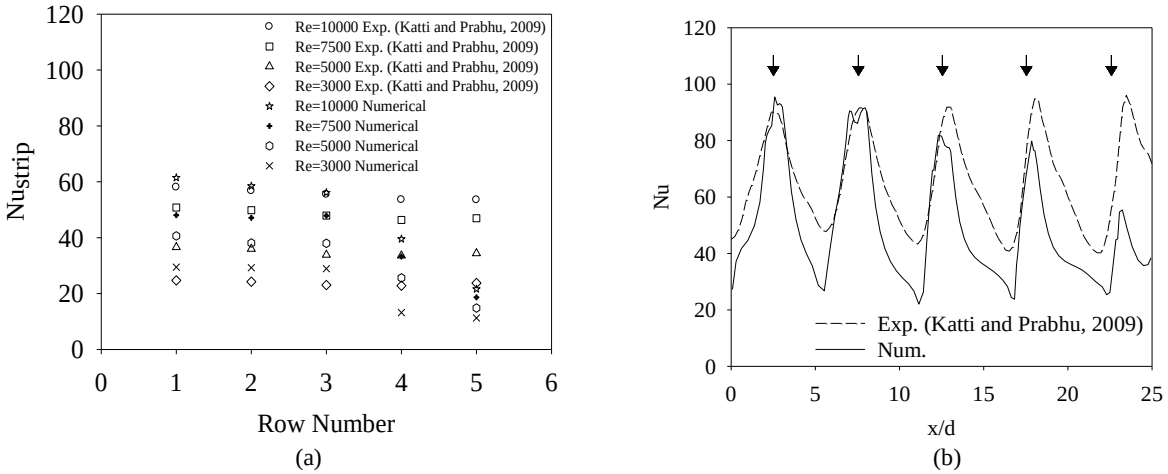

Figure 4. Comparison of numerical results with exp. measurements of Katti and Prabhu (2009) (a) Nu_{strip} values, (b) Local Nu number values

The effect of Re number on the local Nu number on triangular and square ribbed surfaces is shown in Figure 7. Increasing the jet Reynolds number enhances the local stagnation Nusselt number for an individual jet. The impingement heat transfer increases when the jet momentum is augmented, i.e., with increasing Re number.

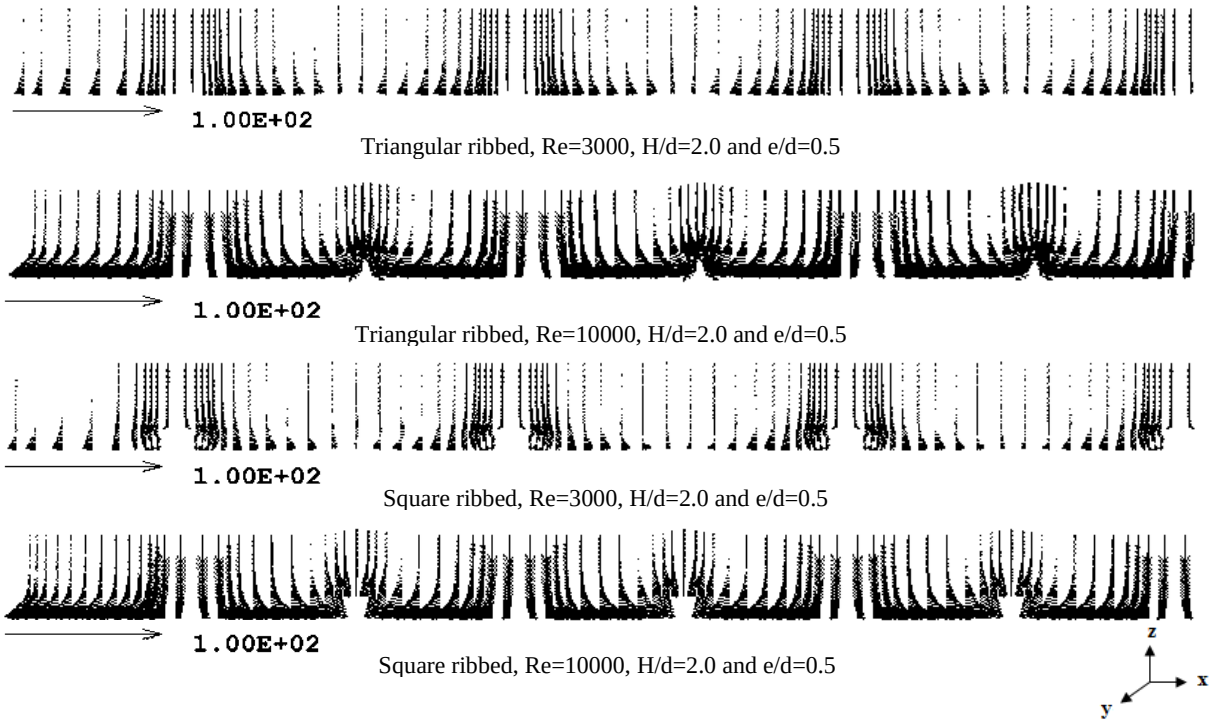

Figure 5. Velocity vectors for triangular and square ribbed surfaces at the mid-plane jet row

It is observed that with increasing Re number the difference between the stagnation point Nu number and the Nu number value at the midsection of two neighboring jets increases. This is attributed to the fact that the wall jets at higher Re numbers impinge more effectively which in turn decreases the velocity and heat transfer rapidly. The Nu number values at the stagnation points are the regions where the maximum heat transfer is achieved, and the regions between the jets are the minimum heat transfer areas. At higher Re numbers the decrease in heat transfer between two jets is higher than at lower Re numbers. One can also see that the Nu number distribution for lower Re numbers is more uniform.

Similar results were obtained for the square ribbed surfaces. However, the Nu number values at the stagnation points rapidly decrease, and minimum values are observed at these points. The maximum Nu number values are obtained at the vicinity of the stagnation points. The heat transfer at the stagnation points has almost the same values with the regions between jets.

Nusselt number contour maps are presented for triangular ribbed surfaces at Re=3000 and Re=10000 at H/d=2.0 and e/d=0.5 in Figure 6 (c) and (d), respectively. As mentioned before, the Nu number distribution is more uniform, and is less affected by the ribs for Re=3000. The Nu number distributions at the stagnation points have a rectangular and elongated shape, in comparison with impinging jet arrays over flat surfaces from the literature (Katti and Prabhu, 2008, 2009a, 2009b; Caliskan and Baskaya, 2012).

Similarly, Nusselt number contour maps are presented for square ribbed surfaces at Re=3000 and 10000 at H/d=2.0 and e/d=0.5 in Figure 7 (e) and (f), respectively. As mentioned before, it can be clearly observed from the Nu number contour maps that the maximum heat transfer was achieved in the vicinity of the stagnation points. The rapid decline in the Nu number values at the stagnation points can also be seen from the contour maps.

Another important parameter which affects the heat transfer of impinging jets is the jet-to-plate distance. There have been many studies performed and available in the literature for different jet-to-plate distances (Lyttle and Webb, 1994). The effect of jet-to-plate distance on the local Nu number on triangular and square ribbed surfaces is presented in Figure 8. The highest stagnation Nu number values for the triangular ribbed case were achieved for H/d=4.0. This is attributed to the potential core region which has generally a length between 4d and 6d. The length of the potential core region is dependent on the turbulence intensity and the initial velocity profile (Geers, 2003). It was observed that the Nusselt numbers for H/d=2.0 and H/d=6.0 at the stagnation points as well as at the mid of two jets have approximately the same values. However, the stagnation point Nu numbers at the edges of the impingement plate for H/d=6.0 are higher which may be due to smaller interaction with neighboring jets. In addition, it was observed that the heat transfer at the stagnation points in the range of $2 \leq H/d \leq 6$ increase steeper, though this is not the case for H/d=8.0, where the heat transfer at the stagnation points are larger. For the square ribbed case it can be seen that the heat transfer at the stagnation points deteriorates, and the maximum heat transfer occurs in the vicinity of the stagnation points for all H/d. The highest and lowest Nusselt number values are obtained for H/d=6.0. Lowest heat transfer along the plate for both rib geometries was achieved for H/d=8.0. This occurs because the impingement plate is situated beyond the potential core of the jet, and the impingement velocity of the fluid in the stagnation region significantly diminishes with increasing jet-to-plate spacing, due to entrainment of the surrounding air (Robinson and Schnitzler, 2007). Similarly to the triangular ribbed surfaces, an increase in the heat transfer at the edges of the impingement plate is obtained for $H/d \geq 6.0$. For H/d=8.0 the highest heat transfer values are achieved at the jets on the edge of the array.

The influence of the jet-to-plate spacing on the heat transfer of the whole plate can be observed from the contour maps in Figure 8 (c) and (d) for triangular and square ribbed surfaces, respectively. One can see that at higher jet-to-plate distances, the Nusselt number distribution on the plate deteriorates due to the strong jet-jet interaction, where the individual jets lose their identity due to mixing by the large scale structures in the flow. It can be seen that for H/d=8.0 the Nusselt number values at the stagnation points are non-uniform, and are stretched in the transverse direction of the ribs. It is also observed that the highest Nu number values are obtained at the edges of the impingement plate. The increase at the side jets for the square ribbed case can be clearly observed. In addition, the decrease at the stagnation points can be seen in Fig. 8 (d).

Rib arrangement impact on heat transfer was also investigated and results are shown in Figure 9. The results presented before were all for the arrangement A. However, in this part of the study the effect of rib arrangement on heat transfer is presented for both the A and B arrangements.

From Figure 9 (a) it is observed that the stagnation point Nusselt number values for arrangement A are significantly higher than the stagnation point Nusselt numbers for arrangement B. This is due to the fact that the impinging jet for arrangement A can more readily penetrate into the enclosing cavity and impinge on the wall. In addition, a decrease in the Nusselt numbers at the stagnation points for arrangement B was observed and the highest heat transfer was achieved at the vicinity of the stagnation points. For arrangement B the heat transfer of the wall jets at the ribs form a secondary maximum which is not observed for arrangement A. In the region between two neighboring jets the heat transfer for arrangement B is higher, where minimum Nusselt number values are obtained for arrangement A. The increase in the Nusselt number for arrangement B between two neighboring jets is due to the lack of rib interactions of the wall jets, and the formation of a recirculation around the ribs, which has a promoting effect on heat transfer in contrary to arrangement A.

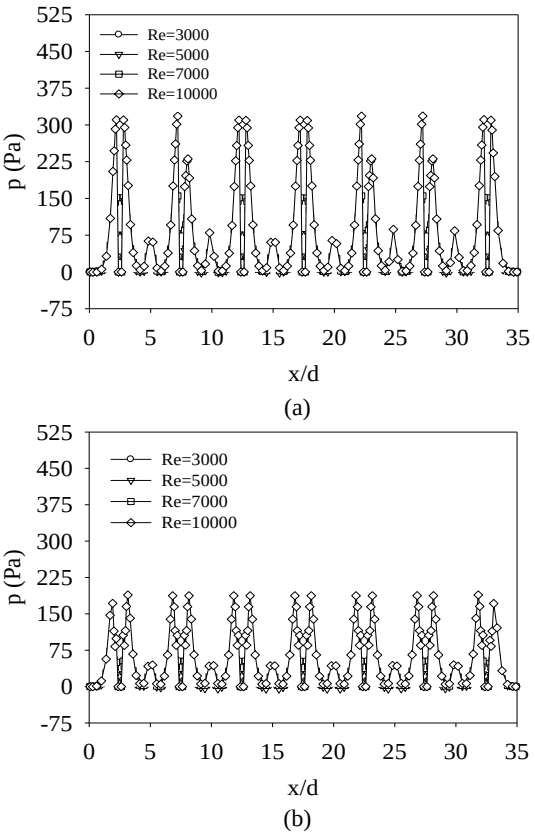

Figure 6. The effect of Reynolds number on the pressure distribution (a) triangular ribbed, (b) square ribbed

In Figure 9 (b) a decrease in the Nusselt number at the stagnation points was observed for both the A as well as the B arrangements. The decrease at the stagnation point for arrangement A is higher than for arrangement B. However, in the vicinity of the stagnation points the decrease is higher for arrangement A. Similarly, to triangular ribbed surfaces, minimum and secondary maximum heat transfer occurs between two neighboring jets for A and B arrangements on square ribbed surfaces, respectively. Rib arrangement effects on the impingement plate was investigated using Nusselt number contour maps, and have been presented in Figure 10. In Figure 10 (a) and (b) Nusselt number contours are shown for Re=3000, H/d=2.0 and e/d=0.5 on triangular and square ribbed surfaces, respectively.

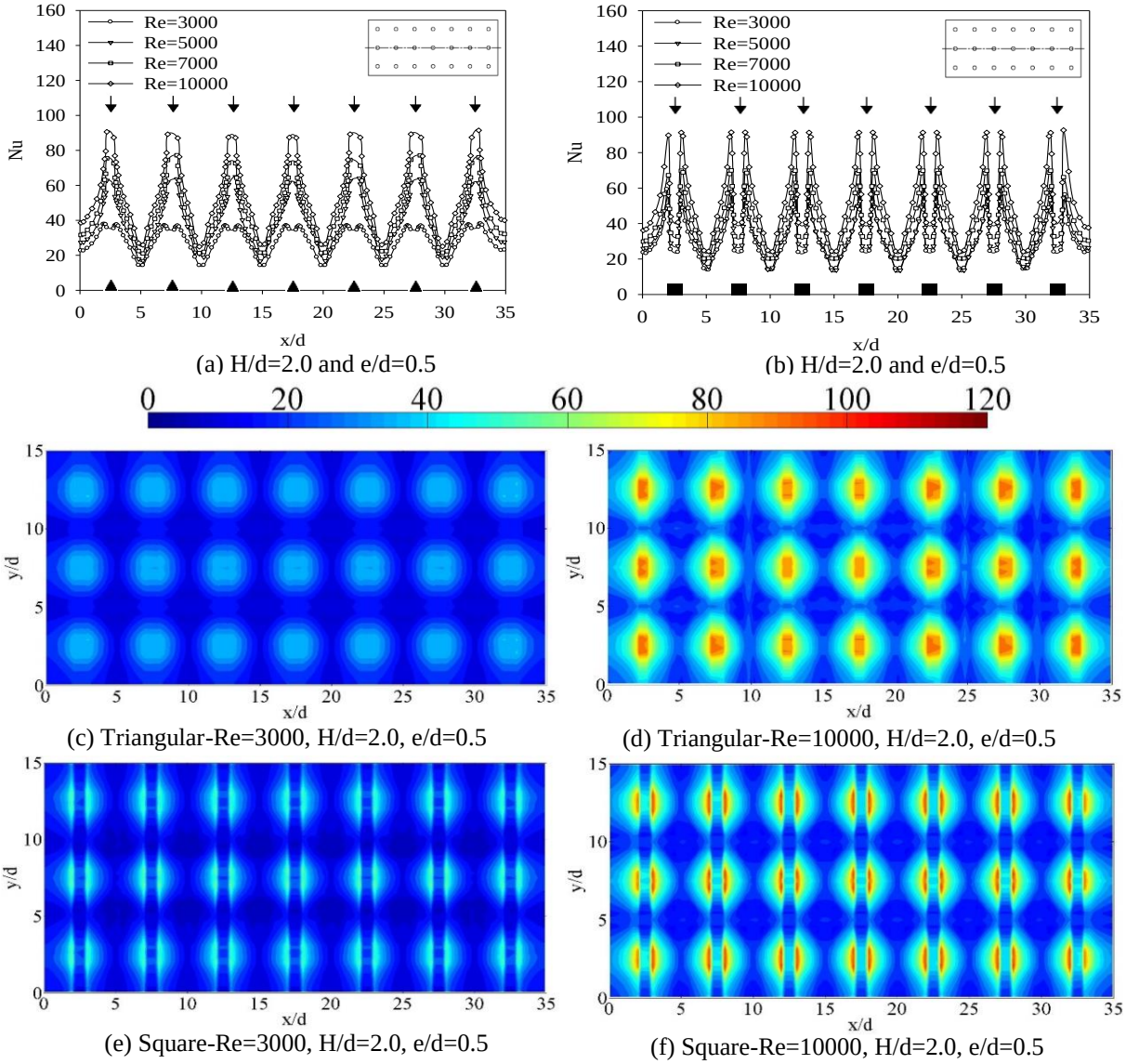

(a) H/d=2.0 and e/d=0.5

(b) H/d=2.0 and e/d=0.5

(c) Triangular-Re=3000, H/d=2.0, e/d=0.5

(d) Triangular-Re=10000, H/d=2.0, e/d=0.5

(e) Square-Re=3000, H/d=2.0, e/d=0.5

(f) Square-Re=10000, H/d=2.0, e/d=0.5

Figure 7. The effect of Reynolds number on the local Nusselt number on triangular and square ribbed surfaces

Nusselt number contours for Re=10000, H/d=2.0 and e/d=0.5 are presented in Figure 10 (c) and (d), respectively. Compared to Re=3000, similar results have been obtained for both the triangular as well as the square ribbed surfaces. However, the heat transfer at the ribbed sections is higher for the square ribbed surfaces. In addition, a decrease in heat transfer at the stagnation points was observed for both the triangular and square ribbed surfaces. The Nu number values in the vicinity of the stagnation points are higher for triangular ribbed surfaces, compared to the square ribbed configuration. In the last two contour maps of Figure 10 the Nu number distributions are shown for Re=10000, H/d=8.0 and e/d=0.5 for triangular and square ribbed surfaces. It can be seen that higher stagnation point Nusselt numbers were obtained on triangular ribbed surfaces. For the square ribbed surface, the stagnation point Nusselt numbers at the two edges in the x-direction are higher than the other stagnation point Nusselt numbers. In addition, for higher jet-to-plate spacing, for arrangement B, the ribs have less effect on heat transfer, especially for the square ribbed surface, where the effect of the ribs is almost unimportant. Compared with arrangement A, deterioration of the stagnation point Nusselt number values at the jet edges was not observed for arrangement B, which was the case for arrangement A at H/d=8.0

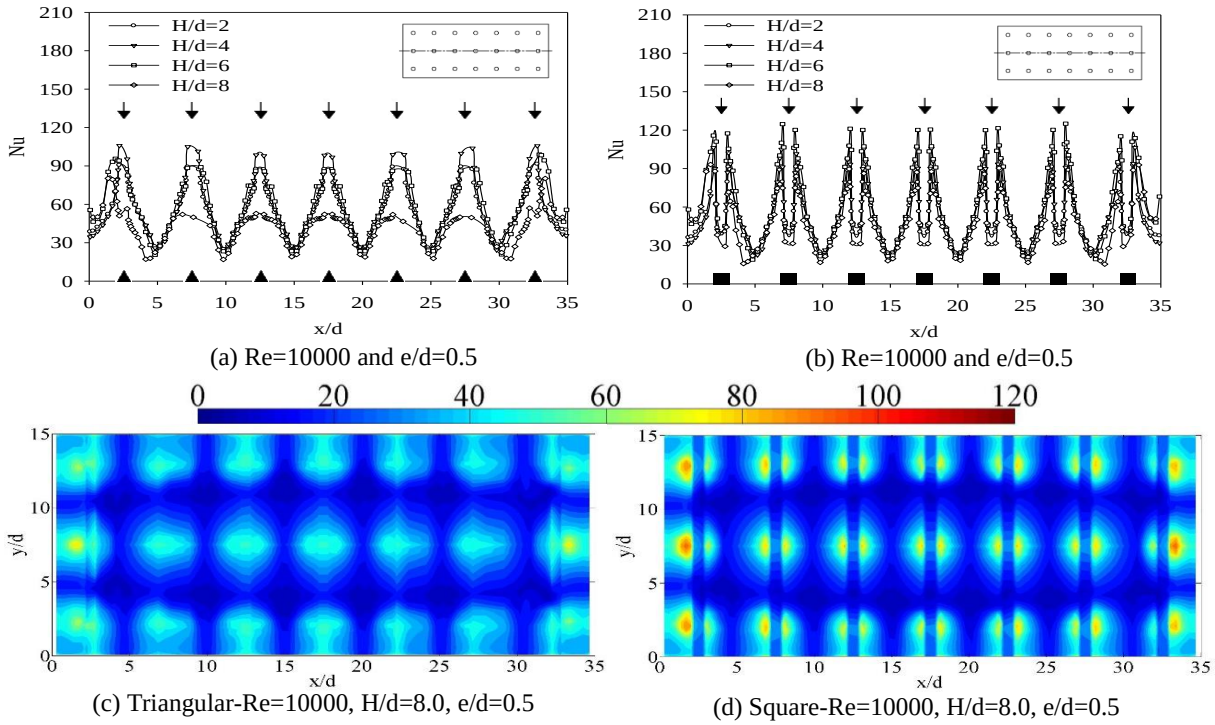

(a) Re=10000 and e/d=0.5

(b) Re=10000 and e/d=0.5

(c) Triangular-Re=10000, H/d=8.0, e/d=0.5

(d) Square-Re=10000, H/d=8.0, e/d=0.5

Figure 8. The effect of H/d on the local Nusselt number on triangular and square ribbed surfaces

In Figure 11 the effect of Reynolds number on the area-averaged Nusselt number is presented for H/d=2.0 and e/d=0.5 on triangular ribbed, square ribbed and smooth surfaces. As an insert, the increase and decrease ratios in heat transfer in comparison to the smooth surface are shown on the same figure. In addition, the results obtained by Caliskan (2013) and Caliskan & Baskaya (2012) are presented. One can see that the results are in good agreement with the literature. The differences between the literature are due to the fact that the studies of Caliskan (2013) and Caliskan & Baskaya (2012) were conducted for a 5 x 3 jet array. It was observed that at Re=3000 the Nusselt number values are almost the same for all cases investigated and the increase ratios are very close. The lowest heat transfer for Re>3000 was obtained with the square ribbed surface with arrangement A. This shows that the ribs in this case have a detrimental effect on momentum, which leads to a decrease in heat transfer. For Re>3000 the highest heat transfer was obtained on the square ribbed surface with arrangement B. Although, in the local Nu number distributions little differences between the arrangements and higher stagnation point values for triangular ribbed surfaces was obtained, it was seen that this is not the case for area-averaged Nu number values, and the arrangement has an unignorable effect on heat transfer. This may be due to the recirculation in the cavities between the ribs where the jets are impinging, and therefore enhancing the heat transfer. For Re>7000 the highest Nu number values were obtained with arrangement B. This may be due to the wall jet interaction which does not occur directly for arrangement B. It can be seen that a decrease in heat transfer occurs at higher Re number values for arrangement A. The highest decrease in heat transfer is observed for Re=10000 on the square ribbed surface with arrangement A, where a decrease of 13.4% is calculated in comparison with the smooth surface. This is due to the decrease in velocity and momentum before impingement of the jets.

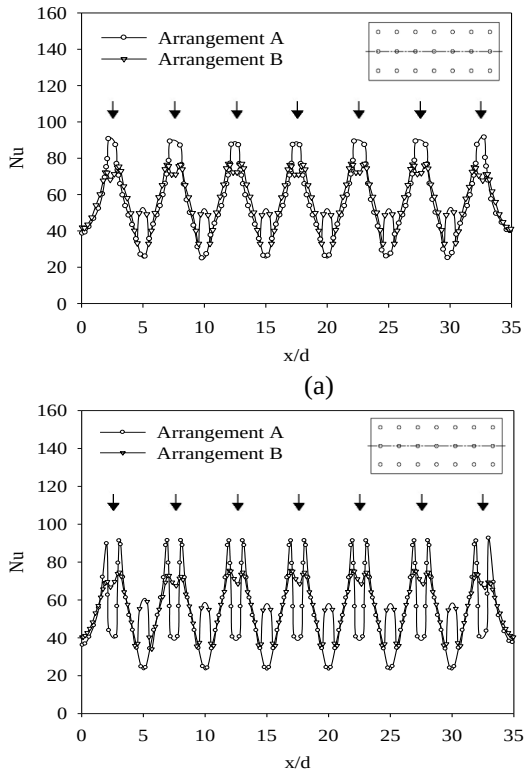

(a)

(b)

Figure 9. The effect of rib arrangement on local Nusselt number under the mid-row jets for Re=10000, H/d=2.0 and e/d=0.5 (a) triangular rib, (b) square rib

In the second figure of Figure 11 the effect of jet-to-plate spacing on the area-averaged Nusselt number is presented for Re=10000 and e/d=0.5. It was observed that the results are in good agreement with the experimental results performed in the mentioned articles. Increase and decrease ratios of heat transfer are also shown in the figure, which

were calculated in comparison with the smooth surface. It was observed that the area-averaged Nusselt number values for all rib geometries with arrangement B are higher at all H/d values compared to arrangement A. It can be seen that the Nu number values for arrangement A are smaller compared with the smooth surface. The highest decrease in heat transfer with 23.1% is obtained for H/d=8.0 on the triangular ribbed surface with arrangement A. This was attributed to the fact that for Re=10000 with arrangement A the interaction of the wall jets have a decreasing effect on the heat transfer. For the ribbed surfaces with arrangement B and the smooth surface, one can see that the heat transfer increases in the range of 2.0≤H/d≤4.0, and the highest Nusselt number values are obtained at H/d=4.0. After H/d>4.0 the heat transfer decreases.

For arrangement B in the range of 2.0≤H/d≤6.0 the highest heat transfer is achieved on the square ribbed surface. The maximum heat transfer is obtained on the square ribbed surface for arrangement B at H/d=4.0. The reason of the highest heat transfer values in this range are attributed to the recirculation in the cavity between ribs, which enhances the heat transfer effectively.

Correlations for the area-averaged Nusselt numbers have been calculated depending on Reynolds number (3000≤Re≤10000), jet-to-plate distance (2.0≤H/d≤8.0), and the dimensionless rib height (0.333≤e/d≤0.667), for triangular and square ribbed surfaces with both A and B arrangements, by a regression analysis. A nonlinear estimation is taken into consideration. The correlations derived for the multiple jet impingements on the triangular and square ribbed surfaces with two different arrangements are given in Eqs. 17-20, respectively. The numerically observed and predicted values of the area-averaged Nusselt numbers for the triangular and square ribbed surfaces are shown in Fig. 12.

For arrangement A on the triangular ribbed surface:

$$Nu_A = 0.655(Re)^{0.46}(H/d)^{-0.18}(e/d)^{0.02} \quad (17)$$

where the standard deviation of the data is 6.8.

For arrangement B on the triangular ribbed surface:

$$Nu_A = 0.213(Re)^{0.58}(H/d)^{-0.1}(e/d)^{0.01} \quad (18)$$

where the standard deviation of the data is 8.1.

For arrangement A on the square ribbed surface:

$$Nu_A = 0.625(Re)^{0.45}(H/d)^{-0.16}(e/d)^{-0.09} \quad (19)$$

where the standard deviation of the data is 6.4.

For arrangement B on the square ribbed surface:

$$Nu_A = 0.262(Re)^{0.57}(H/d)^{-0.13}(e/d)^{0.03} \quad (20)$$

where the standard deviation of the data is 9.5.

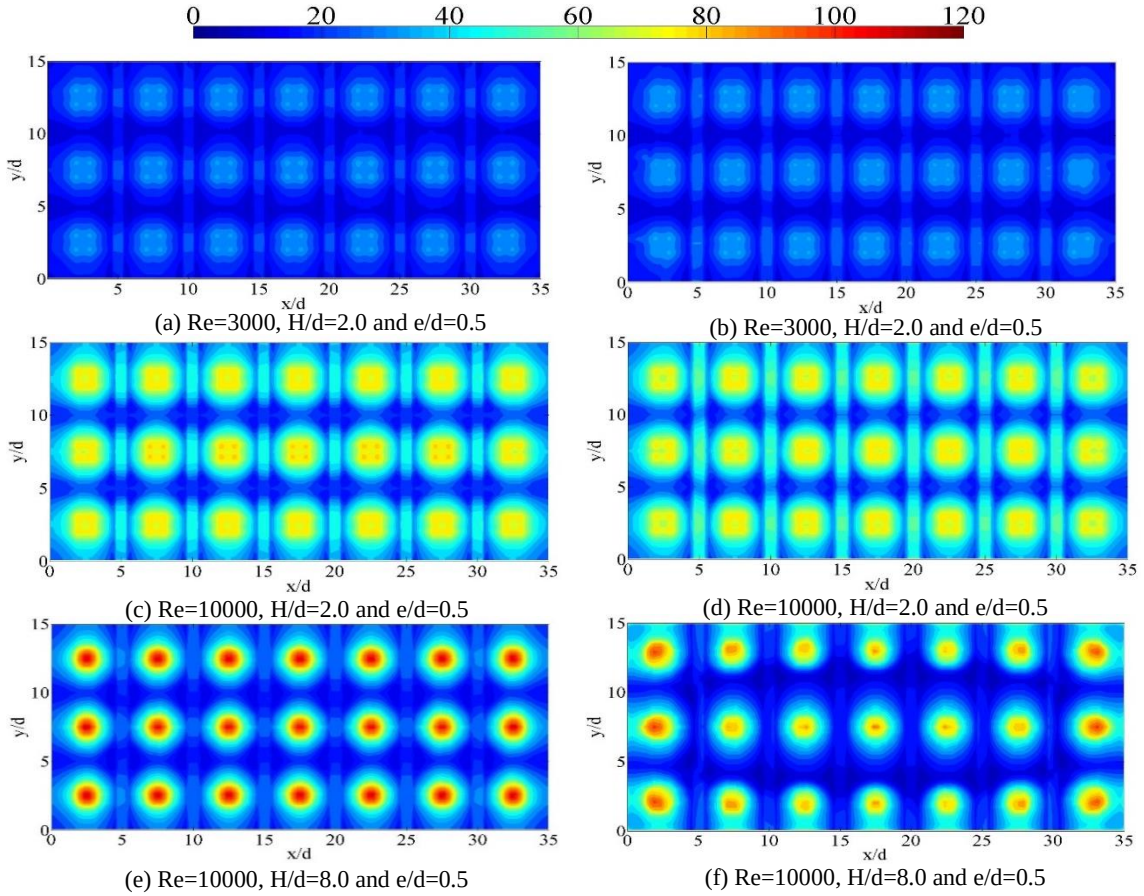

(a) Re=3000, H/d=2.0 and e/d=0.5

(b) Re=3000, H/d=2.0 and e/d=0.5

(c) Re=10000, H/d=2.0 and e/d=0.5

(d) Re=10000, H/d=2.0 and e/d=0.5

(e) Re=10000, H/d=8.0 and e/d=0.5

(f) Re=10000, H/d=8.0 and e/d=0.5

Figure 10. Nusselt number contour maps for arrangement B (a), (c), (e) Triangular ribbed surface and (b), (d), (f) Square ribbed surface

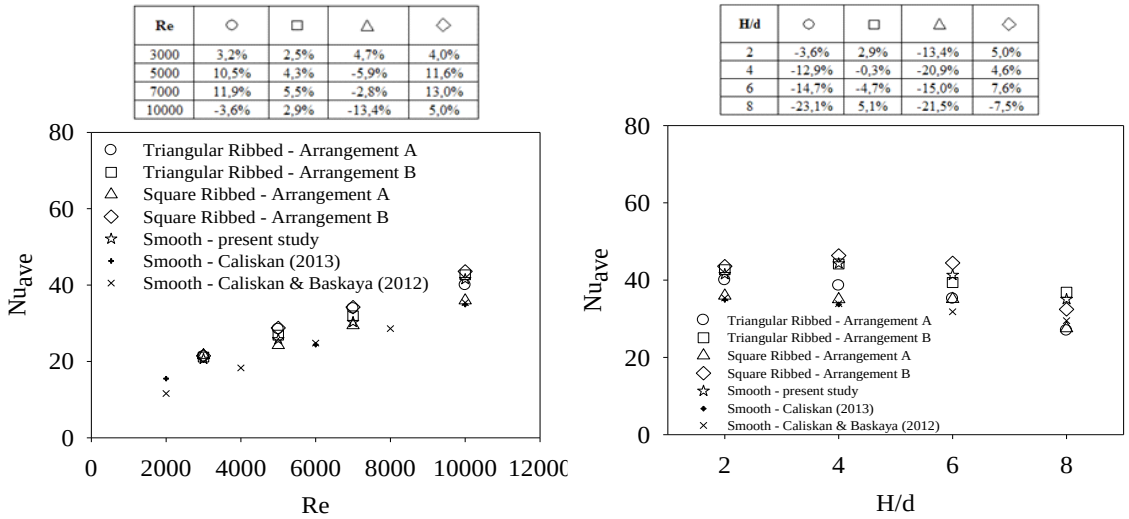

Figure 11. Effect of Reynolds number and H/d on area-averaged Nusselt number for different rib arrangements and rib geometries at e/d=0.5

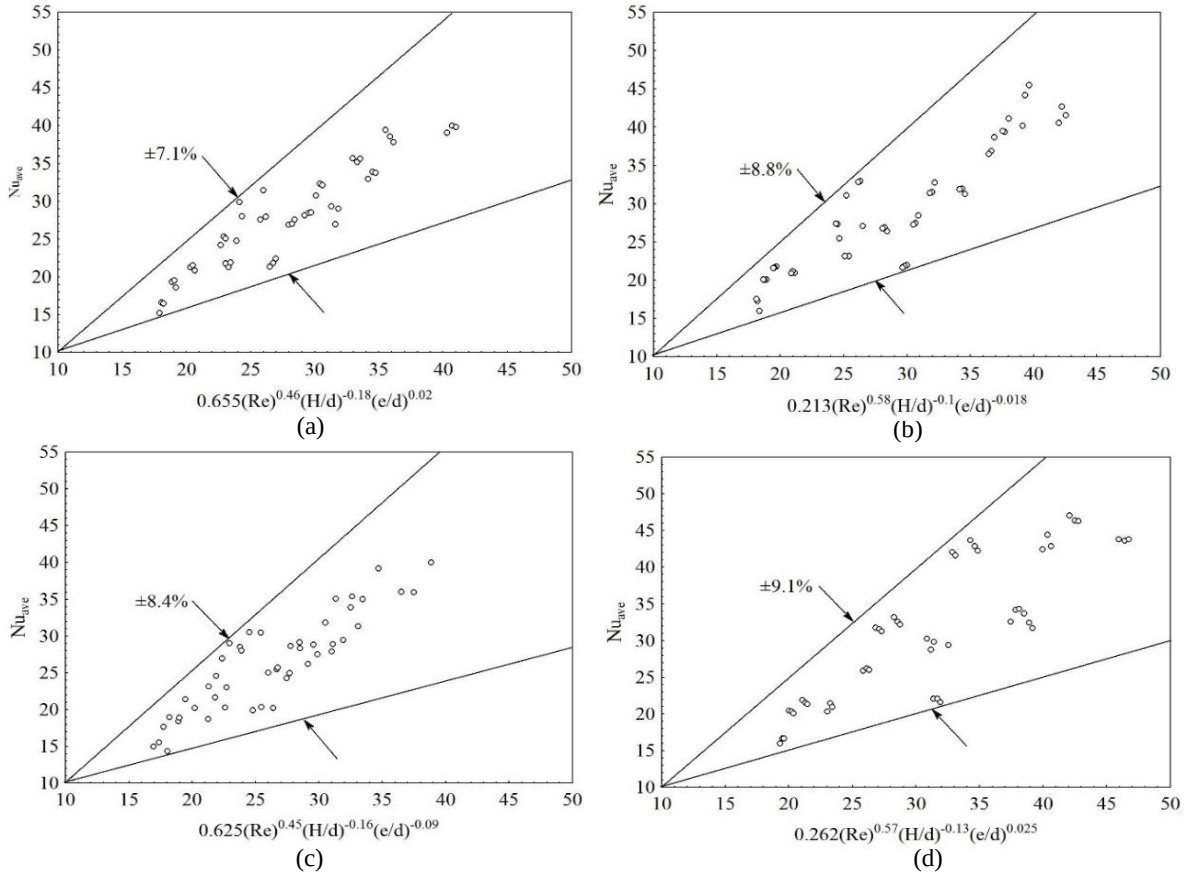

Fig. 12. Correlations of the area-averaged Nusselt number for triangular and square ribbed surface with 3000≤Re≤10000, 2.0≤H/d≤8.0 and 0.333≤e/d≤0.667, (a) Arrangement A-triangular ribbed, (b) Arrangement B- triangular ribbed, (c) Arrangement A-square ribbed, (d) Arrangement B-square ribbed

CONCLUSIONS

Flow field and heat transfer characteristics of a jet array impinging on triangular and square ribbed surfaces for different Re numbers, H/d and two different rib arrangements have been investigated. Local and average Nusselt number distributions were obtained, and the change in the heat transfer was observed, and compared to the results with a smooth wall. Wall jets of neighboring jets have a stronger interaction with increasing Reynolds number. For square ribbed surfaces the local Nusselt number values at the stagnation point rapidly decrease and minimum values are observed at these points. The maximum Nu number values are obtained at the vicinity of the stagnation points. On triangular and square ribbed surfaces, the highest stagnation point Nu number values were achieved for H/d=4.0 and H/d=6.0, respectively. Lowest heat transfer for both rib geometries was obtained for H/d=8.0. On triangular ribbed surfaces the stagnation point Nusselt number values for arrangement A are

significantly higher than the stagnation point Nusselt numbers for arrangement B. On square ribbed surfaces a decrease in the Nusselt number at the stagnation points was observed for both the A as well as the B arrangements.

The highest increase in the area-average Nu compared to the smooth surface was obtained on the square ribbed surface with arrangement B for Re=7000. The effect of jet-to-plate spacing on the area-averaged Nusselt number was shown for Re=10000 and e/d=0.5. The highest decrease in heat transfer in comparison with the smooth surface is obtained for H/d=8.0 on the triangular ribbed surface with arrangement A.

REFERENCES

Bredberg J., Davidson L., 2004, Low-Reynolds Number Turbulence Models: An Approach for Reducing Mesh Sensitivity, *J. of Fluids Engineering, Transactions of the ASME*, 126, 14-21.

Caliskan S., 2013, Flow and Heat Transfer characteristics of transverse perforated ribs under impingement jets, *Int. J. of Heat and Mass Transfer*, 66, 244-260.

Caliskan S., Baskaya S., 2012, Experimental investigation of impinging jet array heat transfer from a surface with V-shaped and convergent-divergent ribs, *Int. J. of Thermal Sciences*, 59, 234-246.

Caliskan S., Baskaya S., Calisir T., 2014, Experimental and numerical investigation of geometry effects on multiple impinging air jets, *Int. J. of Heat and Mass Transfer*, 75, 685-703.

Celik I.B., Ghia U., Roache P.J., Freitas C.J., Coleman H., Raad P.E., 2008, Procedure for estimation and reporting of uncertainty due to discretization in CFD applications, *ASME J. Fluids Eng.*, 130(7), 1-4.

Gau C., Lee I.C., 1992, Impingement cooling flow structure and heat transfer along rib-roughened walls, *Int. J. of Heat and Mass Transfer*, 35(11), 3009-3020.

Gau C., Lee I.C., 2000, Flow and impingement cooling heat transfer along triangular rib-roughened walls, *Int. J. of Heat and Mass Transfer*, 43, 4405-4418.

Katti V., Prabhu S.V., 2008, Influence of spanwise pitch on local heat transfer distribution for in-line arrays of circular jets with spent air flow in two opposite directions, *Experimental Thermal and Fluid Science*, 33, 84-95.

Katti V., Prabhu S.V., 2009, Influence of Streamwise pitch on local heat Transfer distribution for in-line arrays of circular jets with spent air flow in two opposite directions, *Experimental Heat Transfer*, 22, 228-256.

Katti V., Prabhu S.V., 2009, Influence of streamwise pitch on the local heat transfer characteristics for in-line arrays of circular jets with crossflow of spent air in one direction, *Heat Mass Transfer*, 45, 1167–1184.

Koseoglu M.F., Baskaya S., 2010, The role of jet inlet geometry in impinging jet heat transfer, modeling and experiments, *Int. J. of Thermal Sciences*, 49, 1-10.

Lytle D., Webb B.W., 1994, Air jet impingement heat transfer at low nozzle-plate spacings, *Int. J. Heat Mass Transfer*, 31(12), 1687-1697.

Patel V.C., Rodi R.W., Scheuere G., 1985, Turbulence models for near wall and low Reynolds number flows: a review, *AIAA Journal*, 23, 1308-1319.

Robinson A.J., Schnitzler E., 2007, An experimental investigation of free and submerged miniature liquid jet impingement heat transfer, *Experimental Thermal and Fluid Science*, 32, 1-13.

San J.Y, Lai M.D., 2001, Optimum jet-to-jet spacing of heat transfer for staggered arrays of impinging air jets, *Int. J. of Heat and Mass Transfer*, 44, 3997-4007.

San J.Y., Shiao W.Z., 2006, Effects of jet plate size and plate spacing on the stagnation Nusselt number for a confined circular air jet impinging on a flat surface, *Int. J. of Heat and Mass Transfer*, 49, 3477–3486.

Wang S.J., Mujumdar A.S., 2005, A comparative study of five low Reynolds number k–ε models for impingement heat transfer, *Applied Thermal Engineering*, 25, 31-44.

Wang T., Lin M., Bunker R.S., 2005, Flow and heat transfer of confined impingement jets cooling using a 3-D transient liquid crystal scheme, *Int. J. of Heat and Mass Transfer*, 47, 4887-4903.